KAGRA Actuator Noise Modeling Report

Yuta Michimura

October 30, 2015

1 Introduction

This report is to summarize the results of actuator noise modeling for the KAGRA suspensions. The modeling was done by using MATLAB Simulink based NoiseBudget script made by Chris Wipf [1].

The main script and the model for the actuator noise modeling are as follows:

- https://granite.phys.s.u-tokyo.ac.jp/svn/LCGT/trunk/kagranoisebudget/Suspensions/run_SAS_NB.m
- https://granite.phys.s.u-tokyo.ac.jp/svn/LCGT/trunk/kagranoisebudget/Suspensions/SAS.slx

You will also need `findNbSVNroot.m`, `myzpk.m`, `plotdobe.m`, and `plotspectrum.m` in the same directroy to run the script.

The main purpose of this modeling is to check if the actuator noise meet the displacement noise requirement set by MIF group, and to check if the feedback signals to the actuators does not saturate DACs. Small actuation efficiency gives less displacement noise, but it requires more feedback voltage.

Although this script works similarly for all suspensions, here I plot the results mainly for BS (Type-B suspension). Actuator design for ITM/ETMs is not fixed yet at this point.

2 Model

The Simulink model is shown together with the transfer functions and noises used for the simulation.

2.1 Simulink model

The actuator noise Simulink model is shown in Fig. 1. We had to use some tricks to simulate out-of-loop stability and feedback signal with Simulink NoiseBudget blocks, `NbNoiseCal` and `NbNoiseSink`. FlexTf is used for suspension transfer functions (light purple blocks) to use frequency response data (`frd`). Seismic noise from vertical coupling is also included in the model.

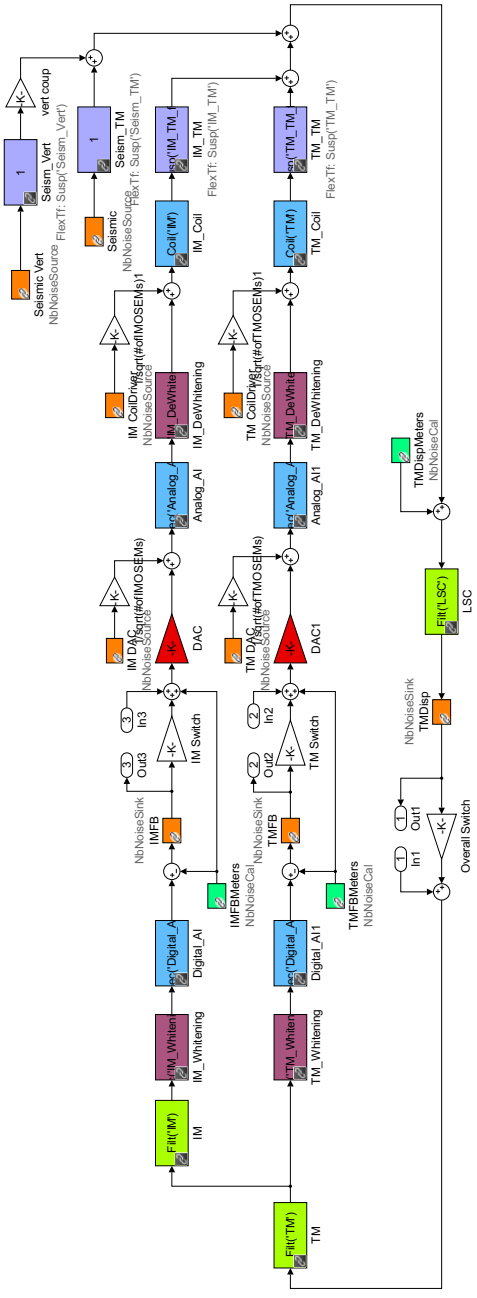

Figure 1: Actuator noise Simulink model.

2.2 Summary of KAGRA Suspensions

KAGRA suspension configurations are summarized graphically in Ref. [2]. For longitudinal degrees of freedom, we basically have actuators for IP (inverted pendulum), IM (intermediate mass), and TM (test mass).

Table 1 is the summary of the actuation for each suspension. Actuation efficiency for a Type-B/Bp coil in N/A is from Ref. [2]. Actuation efficiency for a Type-C TM coil are estimated from the measurement done in June 2015 [6]. The measurement for MCe gives 6.9×10^{-6} m/V at DC, and this gives 1.1×10^{-4} N/V assuming IMC mirror mass to be 0.47 kg and the resonant frequency to be 0.94 Hz. The V-I conversion of coil driver for IMC mirrors is 20 mA/V (50 Ω) [7], so this means the actuation efficiency for a Type-C TM coil is 1.4×10^{-3} N/A (this is consistent with Y. Fujii's coil-magnet coupling measurement [8]).

Table 1: KAGRA suspension actuator parameters. The TM/IM masses and wire lengths for Type-B/Bp suspensions come from Ref. [3]. Those for Type-A suspensions come from Ref. [4]. Those for Type-C suspensions come from private communication with K. Arai, R. Takahashi, and T. Saito. TM actuation efficiency for Type-C comes from Ref. [6].

Type	Type-A	Type-B (BS)	Type-B (SR)	Type-Bp	Type-C
Applicable mirrors	ITM,ETM	BS	SRM,SR2,SR3	PRM,PR2,PR3	MCi,MCo,MCe
Mirror diameter	$\phi = 220$ mm	$\phi = 370$ mm	$\phi = 250$ mm	$\phi = 250$ mm	$\phi = 95.95$ mm
Mirror thickness	150 mm	80 mm	100 mm	100 mm	29.5 mm
Mirror substrate	Sapphire	Fused Silica	Fused Silica	Fused Silica	Fused Silica
Mirror mass	22.7 kg	18.9 kg	10.8 kg	10.8 kg	0.47 kg
Intermediate Mass mass	53.2 kg	36.5 kg	15.6 kg	15.6 kg	0.71 kg
Wire length between TM and IM	0.3 m	0.5 m	0.5 m	0.5 m	0.25 m
Wire length between IM and Platform/BF	0.4 m	0.5 m	0.5 m	0.5 m	0.25 m
TM actuation per coil [N/A]	??	0.129	0.129	0.129	1.4×10^{-3}
# of TM coils for long.	4	4	4	4	4
IM actuation per coil [N/A]	??	1.12	1.12	1.12	N.A.
# of IM coils for long.	??	1	1	1	0

2.3 Suspension transfer functions

For the suspension transfer functions, the ones simulated with SUMCON developed by T. Sekiguchi [11] were used.

The example suspension transfer functions from actuation on IM/TM (from respective recoil masses) to TM displacement are shown below.

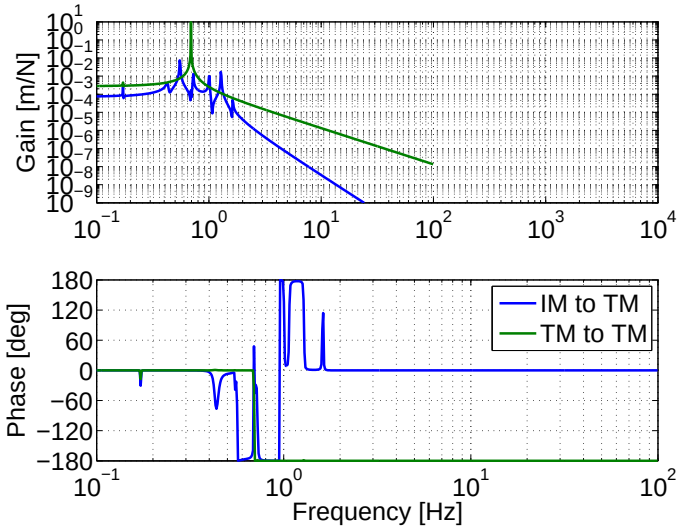

Figure 2: BS suspension transfer functions.

The exmaple seismic noise supression ratio are shown below. The vertical one is also plotted. The vertical to longitudinal coupling was assumed to be 1% in the modeling.

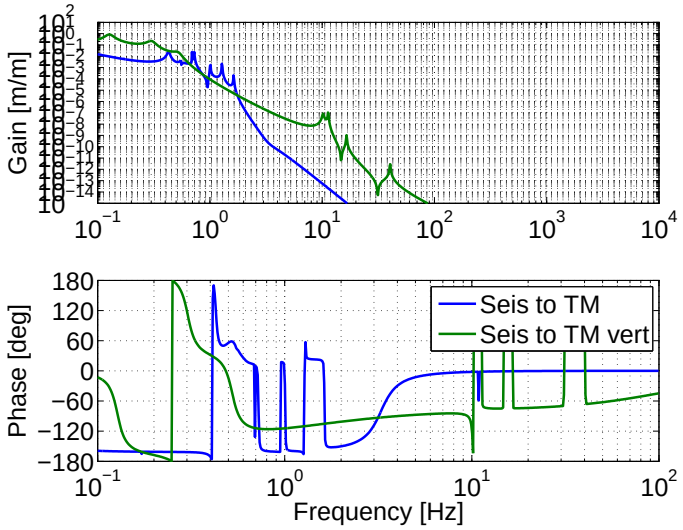

Figure 3: BS seismic noise supression ratio.

2.4 Seismic noise

The Kamioka seismic noise used in the modeling is plotted below. The data is taken on a very noisy day to model the worst case scenario. See Ref. [12] for more detailed seismic noise study.

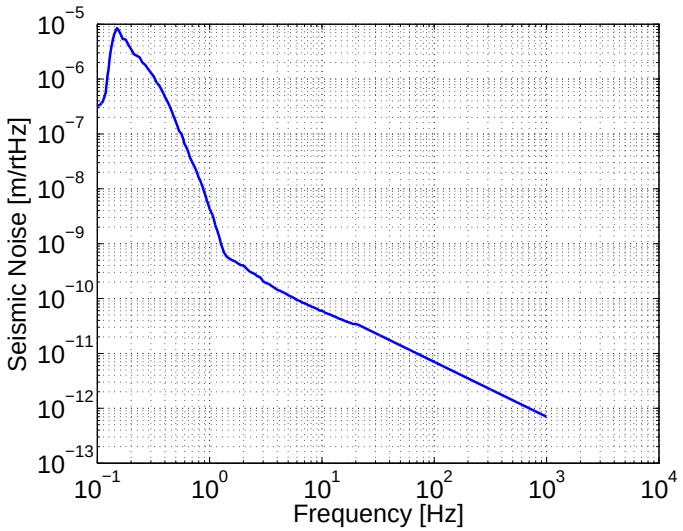

Figure 4: Kamioka seismic noise.

2.5 Coil drivers

We have two types of coil drivers, the high power one and the low power one. They are basically the copies of LIGO-D0902747 and LIGO-D070481, respectively, but has different dewhitening filters compared with LIGO ones. The schematics of the high power coil driver and the low power coil driver are in Ref. [9] and Ref. [10], respectively, and the resistances are 80 Ω for the high power one, and 7.8×10^3 Ω at DC for the low power one. The high power one and the low power one both have switchable three-stage dewhitening filters with pole @ 1 Hz and zero @ 10 Hz (gain of 1 at DC). In the simulation, all the dewhitening filters are turned on.

The low power ones are used for both IM and TM coils. V-I conversion factor for the coil driver when all the dewhitening filters are turned off is plotted in Fig. 5. The resistance of the coil is not included here, but it is included in the model (as 13 Ω).

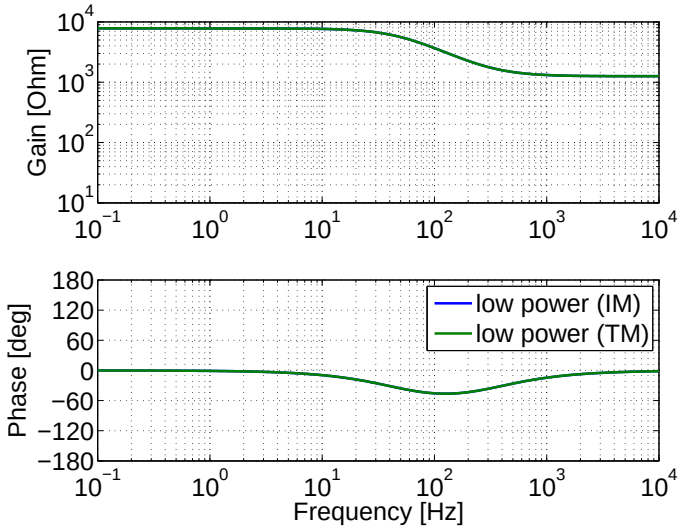

Figure 5: Inverse of V-I conversion factors for IM and TM.

The transfer functions of the whitening and the dewhitening filters are plotted below.

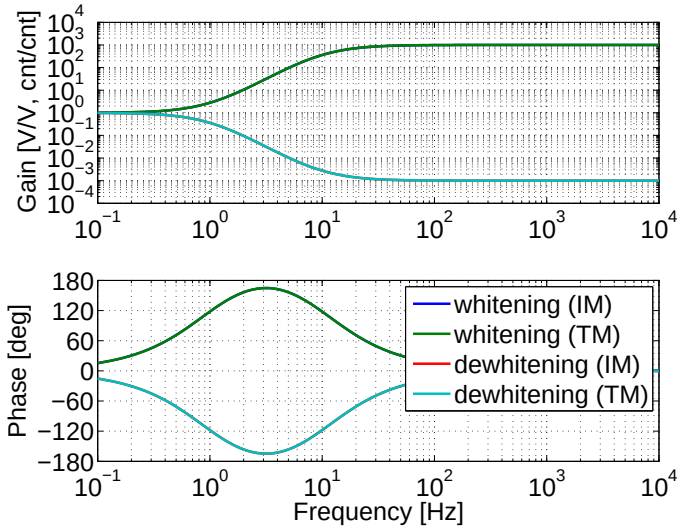

Figure 6: Whitening and dewhitening filters for IM and TM.

Noises of coil drivers used in the model are plotted below, as input equivalent noise to the V-I conversion stage. The spectra come from LIGO-T0900233.

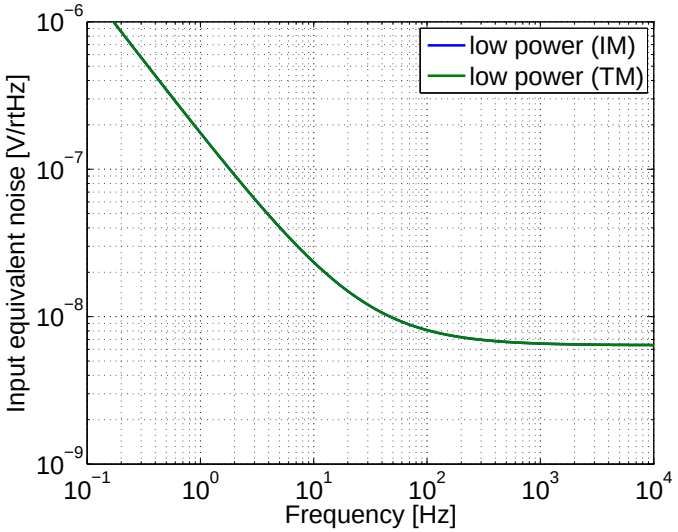

Figure 7: Input equivalent coil driver noise spectra.

2.6 DAC

The DAC used for KAGRA is 16 bit and has the range of ±10 V. So, the least square bit for the DAC is 20 V/2^16 cnts = 0.305 mV/cnts. The DAC noise is plotted below.

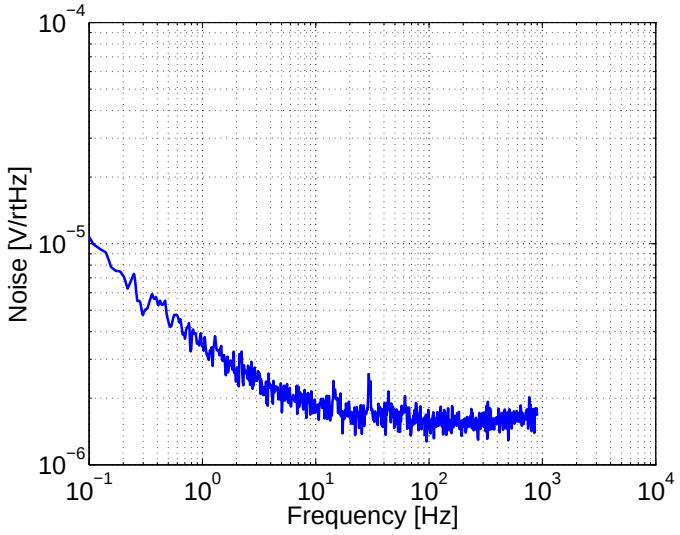

Figure 8: DAC noise.

3 Results for BS

Resulting plots for BS actuator noise modeling are shown. BS is suspended by a Type-B suspension, but differs from other Type-B's since the mirror mass is heavier.

3.1 Openloop transfer function

The openloop transfer funtion is shown below.

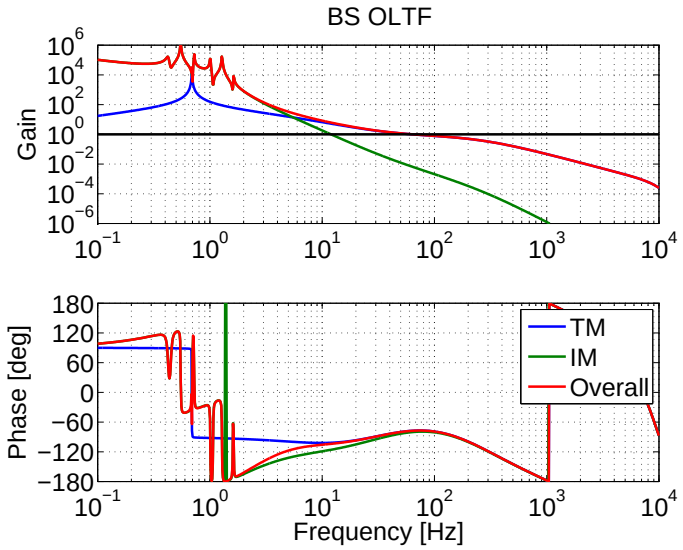

Figure 9: Openloop transfer functions for the BS length servo.

3.2 Noise budget

The displacement noise budget and the actuator noise budget are shown below. The lines labeled "Requirement" show the BS displacement noise requirement in Ref. [13], and the safety factor of 10 is included.

As you can see, the seismic noise and the actuator noise barely meet the requirement above 10 Hz. The most contributing noise among the actuator noises is the noise from TM coil driver. It is desirable to reduce the actuation efficiency for BS TM. Considering the magnetic noise, using smaller magnets is the best way to reduce the actuator noise.

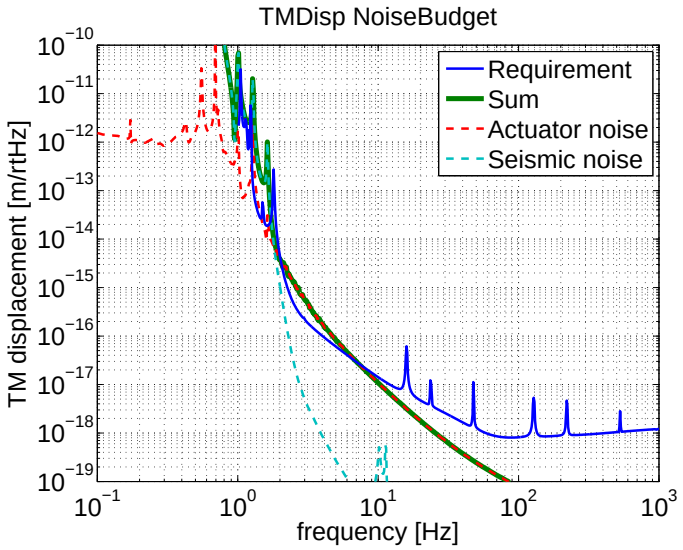

Figure 10: Displacment noise budget for BS.

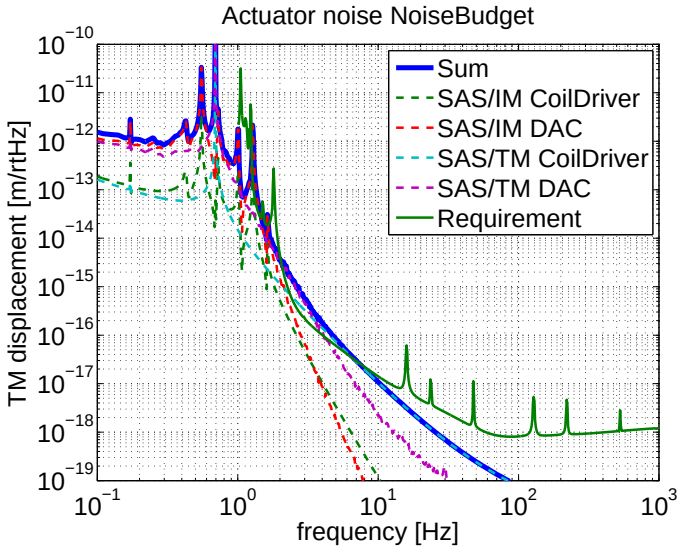

Figure 11: Actuator noise budget for BS.

3.3 Feedback signal saturation check

The spectra of feedback signals for IM and TM are shown in the figures below. The blue lines labeled "DAC limit" shows the DAC range (2^{16}).

As you can see, the RMS's of the feedback signals do not exceed the DAC limit. So, we can reduce the actuation efficiency for BS to be more safe in actuator noise.

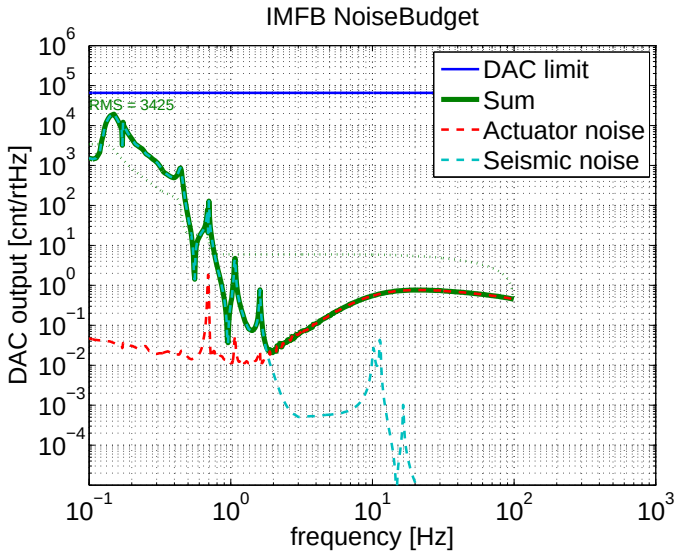

Figure 12: Spectra of feedback signals for the BSIM.

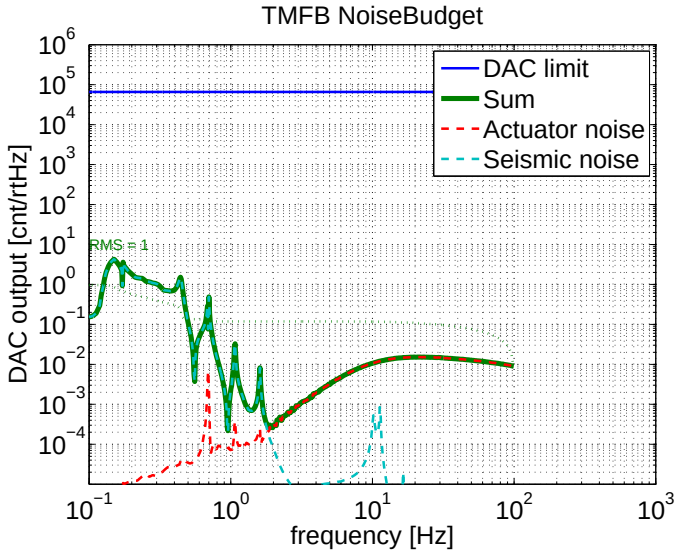

Figure 13: Spectra of feedback signals for the BSTM.

4 Results for SRM

Resulting plots for SRM actuator noise modeling are shown. SRM is suspended by a Type-B suspension. Although displacement noise requirements for SRM and BS is similar, SRM is more severe to the actuator noise since SRM is lighter than BS.

4.1 Noise budget

The displacement noise budget and the actuator noise budget are shown below.

As you can see, the seismic noise meet the requirement above 10 Hz, but the actuator noise does not. The most contributing noise among the actuator noises is the noise from TM coil driver. We should reduce actuation efficiency for SRM TM by more than a factor of 2. Considering the magnetic noise, using smaller magnets is the best way to reduce the actuator noise.

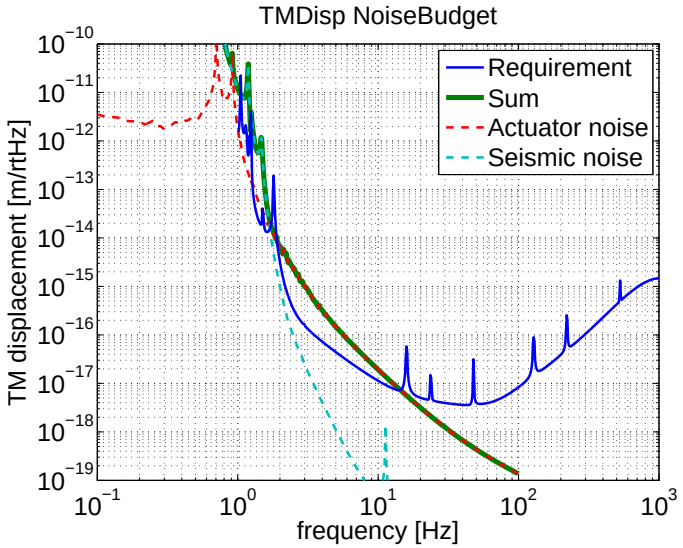

Figure 14: Displacment noise budget for SRM.

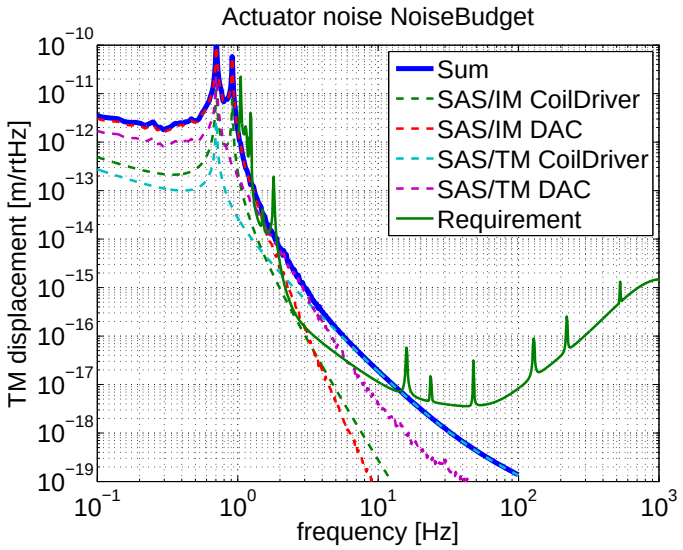

Figure 15: Actuator noise budget for SRM.

4.2 Feedback signal saturation check

The spectra of feedback signals for IM and TM are shown in the figures below.

As you can see, RMS of the feed back signals do not exceed the DAC limit. So, we can reduce the actuation efficiency for SRM to meet the actuator noise requirement.

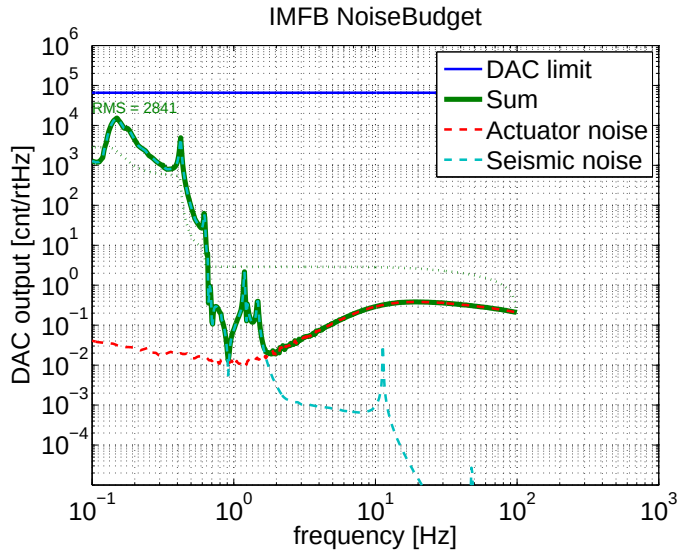

Figure 16: Spectra of feedback signals for the SRMIM.

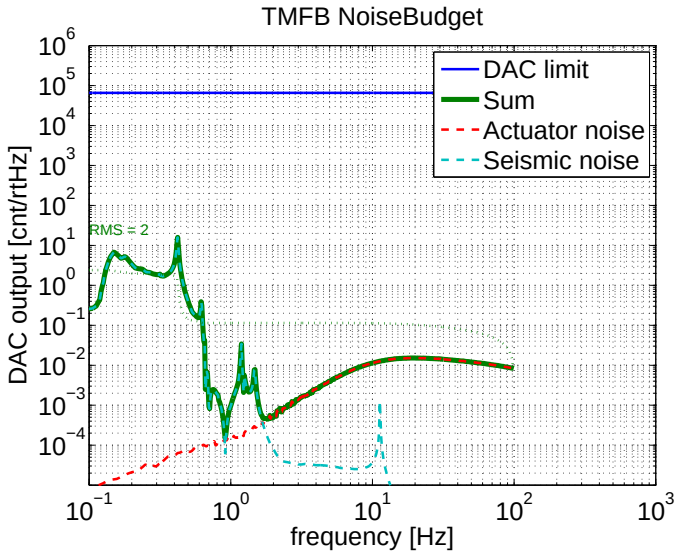

Figure 17: Spectra of feedback signals for the SRMTM.

5 Results for PRM

Resulting plots for PRM actuator noise modeling are shown. PRM is suspended by a Type-Bp suspension. Type-Bp suspension is basically Type-B, but upper stage (Standard Filter) is fixed. So, actuation transfer functions are the same as SRM ones, but seismic suppression ratios are different.

5.1 Noise budget

The displacement noise budget and the actuator noise budget are shown below.

As you can see, the seismic noise and the actuator noise well meet the requirement above 10 Hz.

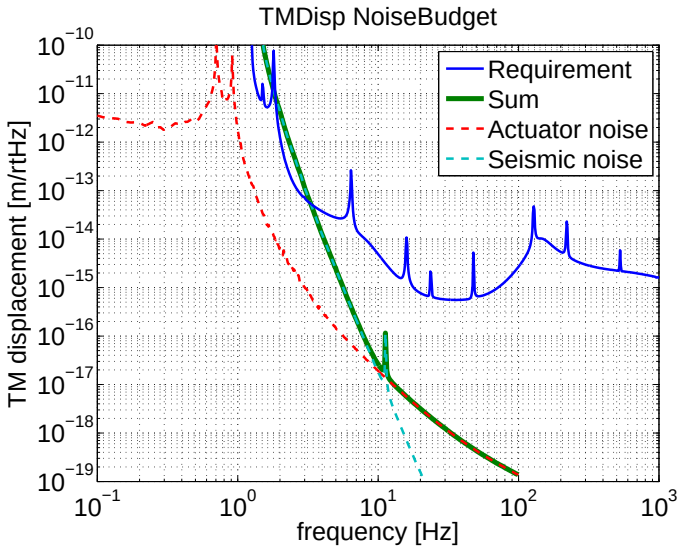

Figure 18: Displacment noise budget for PRM.

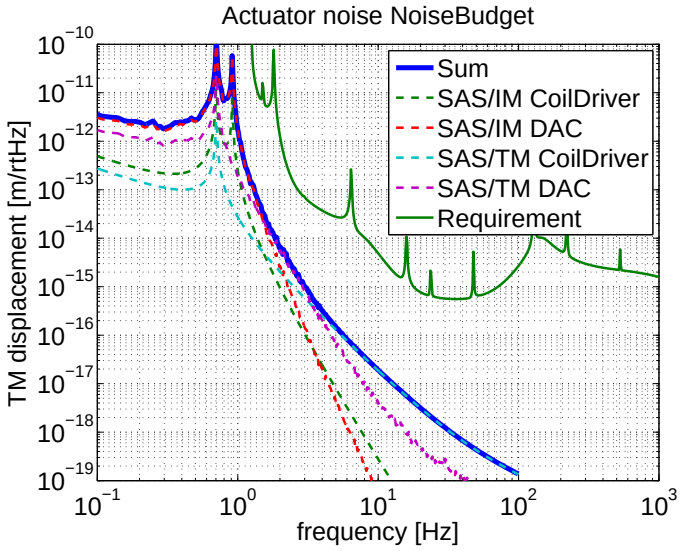

Figure 19: Actuator noise budget for PRM.

5.2 Feedback signal saturation check

The spectra of feedback signals for IM and TM are shown in the figures below.

As you can see, RMS of the feed back signals do not exceed the DAC limit. However, it is very close for IM. So, it is desirable to increase the actuation efficiency for IM. Increasing the actuation efficiency can be done by reducing the resistance of the coil driver.

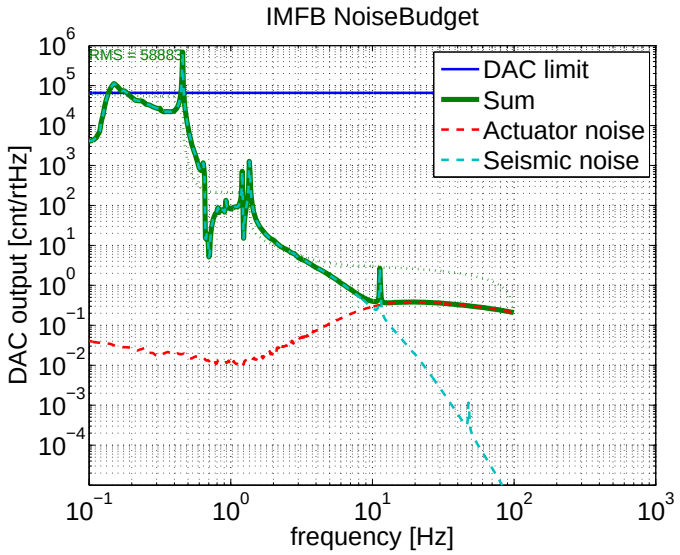

Figure 20: Spectra of feedback signals for the PRMIM.

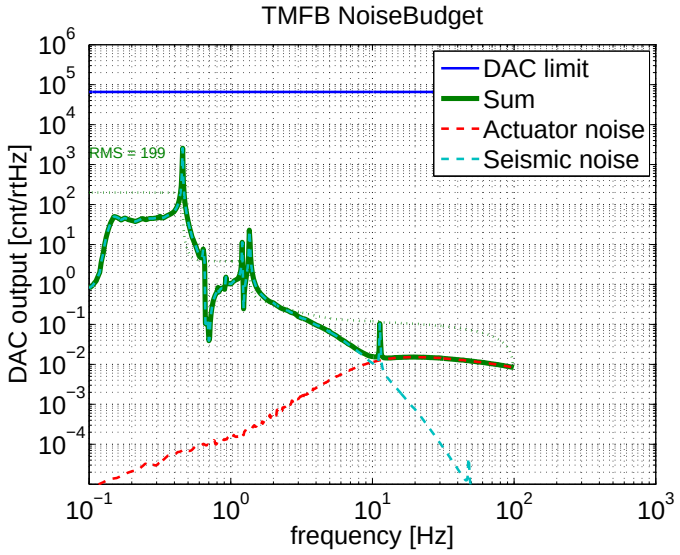

Figure 21: Spectra of feedback signals for the PRMTM.

6 Results for IMC suspensions

Resulting plots for actuator noise modeling for IMC suspensions are shown. IMC mirrors are suspended by Type-C suspension, which is a modified version of the old TAMA PO type suspension. Type-C suspension is a double pendulum fixed on a three-stage stack. There are no actuators for IM. Whitening and

dewhitening filters are not used for coils for IMC suspensions. Coil driver for IMC suspensions are different from Type-B ones, we use TAMA coil drivers described in Ref. [7]. V-I conversion is a flat 50 Ω.

For calculating the vertical motion of IMC mirrors, only the isolation ratio from the double pendulum is used in this modeling. The vertical motion should be smaller than the model since we also have isolation from stacks. The vertical to longitudinal coupling was also assumed to be 1%.

6.1 Noise budget

The displacement noise budget and the actuator noise budget are shown below. The displacement noise requirement for the IMC suspensions comes from the frequency noise requirement after the frequency stabilization servo using IMC length.

As you can see, the seismic noise and the actuator noise well meet the requirement above 10 Hz.

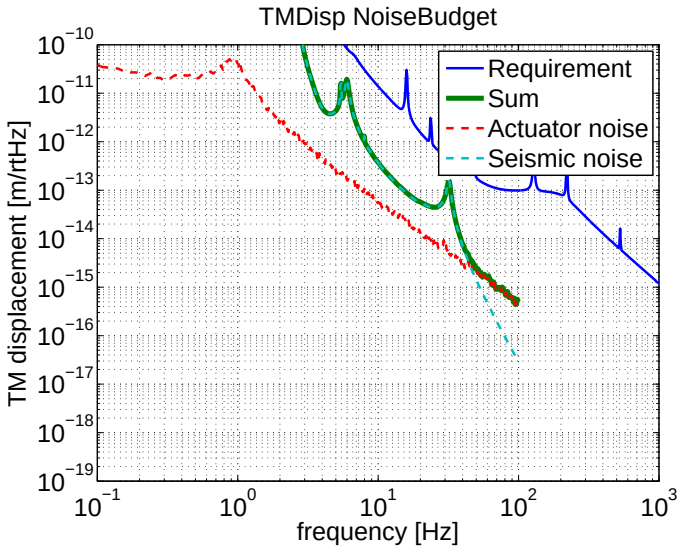

Figure 22: Displacment noise budget for IMC.

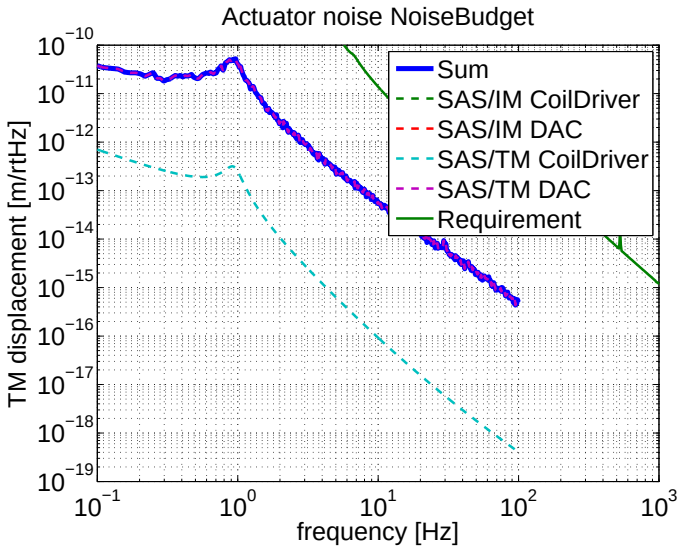

Figure 23: Actuator noise budget for IMC.

6.2 Feedback signal saturation check

The spectra of feedback signals for IM and TM are shown in the figures below.

As you can see, RMS of the feed back signal does not saturate the DAC limit.

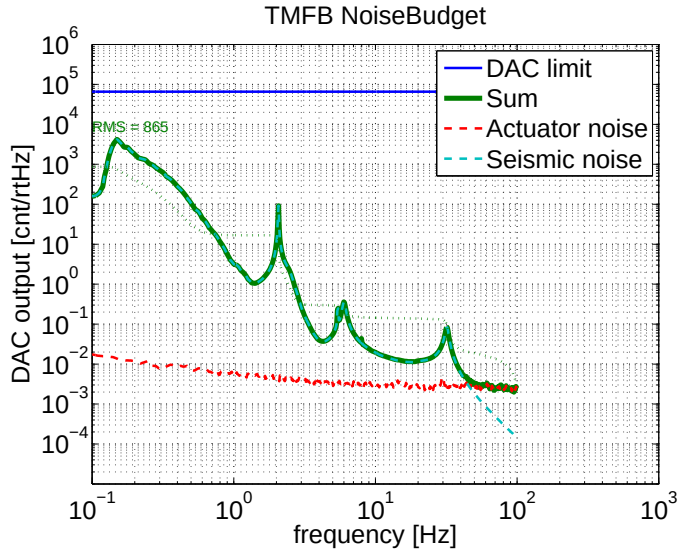

Figure 24: Spectra of feedback signals for the IMCTM.

7 Results for ITM and ETM

To be calculated. Waiting for coil-magnet design.

8 Saturation on lock acquisition

We also have to check if the DAC and the coil drivers do not saturate on lock acquisition. The maximum current the low power coil drivers can produce is 10 mA (AD8671) [10], and that for the coil drivers for IMC is 440 mA (EL2099) [7].

The force we need to stop the TM mirror can be roughly estimated by

$$F = \frac{mv}{\Delta t}, \tag{1}$$

where m and v are the mass and the velocity of the mirror, respectively. Δt is the time it takes to pass the linewidth of the error signal d, and $\Delta t = d/v$. So,

$$F = \frac{mv^2}{d}. \tag{2}$$

The estimation for the force and corresponding current to each coil, voltage to each coil driver (DAC output) are show in Table 2.

Table 2: The force we need to stop mirrors. The velocities for Type-B/Bp suspensions are estimated from the RMS velocities after local damping, simulated by A. Shoda. The velocity for Type-C suspension is estimated using the Matlab code from R. Takahashi.

Mirrors	ITM,ETM	BS	SR	PR	IMC
Type	A	B (BS)	B (SR)	Bp	C
Mass [kg]	22.7	18.9	10.8	10.8	0.47
Velocity [um/sec]	TBD	0.2	0.2	4.4	2.3
Linewidth [nm]	9 (green)	532	14	9	1
Force [N]	TBD	1.4e-6	3.1e-5	2.3e-2	2.5e-3
Coil current [mA]	TBD	0.0028	0.060	45	443
DAC output [V]	TBD	0.022	0.47	351	23

From this study, we can say that;

- We can reduce BS TM actuation efficiency by upto factor of 1/930, by reducing the magnet size.
- We can reduce SRM TM actuation efficiency by upto factor of 1/43, by reducing the magnet size.
- We should use the coil driver with higher power for PRM TM (resistance of less than 440 Ω, output current more than 45 mA).
- It is desirable to increase number of turns or use bigger magnets for IMC.

9 Magnetic noise coupling

We also have to check the magnetic noise coupling for the actuation design study. This calculation for Type-B and Type-Bp suspensions are given in Ref. [14], and we confirmed that the magnetic noise is small enough. However, detailed study is not done yet, and Virgo experience show that the calculation given in Ref. [14] is too optimistic.

Rough estimate for the magnetic noise coupling for the IMC suspensions is 1×10^{-14} m/$\sqrt{\text{Hz}}$ at 10 Hz, and this is three orders of magnitude smaller than the displacement noise requirement. For IMC mirrors, four NdFeB magnets (diameter 1 mm, length 12 mm) are attached and here I assumed the magnetic moment to be 0.0083 J/T for a magnet. Also, the common mode rejection of 1/100 is assumed.

10 Summary

- It is desirable for BS TM to have smaller magnets (by factor of about 1/900).
- SRM TM should have smaller magnets (by factor of about 1/40).
- It is desirable for the coil driver for PRM IM to have smaller resistance.
- The coil driver for PRM TM should be high power (resistance of less than 440 Ω, output current more than 45 mA).
- It is desirable to increase number of turns or use bigger magnets for IMC.
- Calculation to be done for ITM and ETM.

References

[1] The source code is available from
https://svn.ligo.caltech.edu/svn/aligonoisebudget.
Some instructions are given at
https://awiki.ligo-wa.caltech.edu/aLIGO/NoiseBudget.

[2] Yuta Michimura: Summary of Suspension Configurations, JGW-D1503415.
http://gwdoc.icrr.u-tokyo.ac.jp/cgi-bin/DocDB/ShowDocument?docid=3415

[3] Riccardo DeSalvo: Recycler and Beam Splitter suspension structure, JGW-T1100571.
http://gwdoc.icrr.u-tokyo.ac.jp/cgi-bin/DocDB/ShowDocument?docid=571

[4] Takanori Sekiguchi: Type-A SAS Mechanical Model Parameters, JGW-T1302090.
http://gwdoc.icrr.u-tokyo.ac.jp/cgi-bin/DocDB/ShowDocument?docid=2090

[5] Mark Barton: OSEM Coil/Magnet/Flag Calculation, JGW-T1503239, Table 1.
http://gwdoc.icrr.u-tokyo.ac.jp/cgi-bin/DocDB/ShowDocument?docid=3239

[6] Yuta Michimura *et al.*: MCe の並進アクチュエータ伝達関数の測定 (6/25-26) on IOO blog.
http://gwclio.icrr.u-tokyo.ac.jp/lcgtsubgroup/inoutoptics/2015/06/mce625-26.html

[7] Gerhard Heinzel: TAMA coil driver modification (2000).
http://tamago.mtk.nao.ac.jp/tama/ifo/general_lib/circuits/000414_coil_driver/coildrv.pdf

[8] Yoshinori Fujii: coil-magnet coupling measurement, JGW-T1503605.
http://gwdoc.icrr.u-tokyo.ac.jp/cgi-bin/private/DocDB/ShowDocument?docid=3605

[9] Masahiro Kamiizumi: High Power Coil Driver Board, JGW-D1503503.
http://gwdoc.icrr.u-tokyo.ac.jp/cgi-bin/private/DocDB/ShowDocument?docid=3503

[10] Masahiro Kamiizumi: Low Power Coil Driver Board, JGW-D1503507.
http://gwdoc.icrr.u-tokyo.ac.jp/cgi-bin/private/DocDB/ShowDocument?docid=3507

[11] The SUMCON is available from the KAGRA SVN;
https://granite.phys.s.u-tokyo.ac.jp/svn/LCGT/trunk/VIS/sumcon

[12] Takanori Sekiguchi: Seismic Spectrum in Kamioka Mine, JGW-T1402971.
http://gwdoc.icrr.u-tokyo.ac.jp/cgi-bin/DocDB/ShowDocument?docid=2971

[13] Yoichi Aso, Yuta Michimura, Kentaro Somiya: KAGRA Main Interferometer Design Document, JGW-T1200913, Figure 4.1 and 4.2.
http://gwdoc.icrr.u-tokyo.ac.jp/cgi-bin/DocDB/ShowDocument?docid=913

[14] Kenji Ono: Evaluation of BS and RM noise arisen from the AC component of geomagnetism field, JGW-T1503469.
http://gwdoc.icrr.u-tokyo.ac.jp/cgi-bin/DocDB/ShowDocument?docid=3469